Diffractive broadband coupling into high-Q resonant cavities

Hongtao Lin,[1] Xiaochen Sun,[2] Jifeng Liu,[3] and Juejun Hu[4,*]

[1]*Department of Materials Science & Engineering, University of Delaware, Newark, Delaware 19716, USA*

[2]*LaXense Inc., 20539 E Walnut Dr. N, Walnut, California 91789, USA*

[3]*Thayer School of Engineering, Dartmouth College, 14 Engineering Drive, Hanover, New Hampshire 03755, USA*

[4]*Department of Materials Science & Engineering, Massachusetts Institute of Technology, 77 Mass. Ave., Cambridge, Massachusetts 02139, USA*

**Corresponding author: hujuejun@mit.edu*

Received March 19, 2015; revised April 25, 2015; accepted April 28, 2015; posted April 30, 2015 (Doc. ID 236514); published May 14, 2015

Optical resonators with high-quality factors (Q-factor) constitute the main building block for many photonic devices capitalizing on light–matter interactions, ranging from light emitters to biochemical sensors. While a high Q-factor enhances light–matter interactions, it also limits the device operation bandwidth. Here we propose and numerically analyze a generic coupling scheme to overcome the apparent trade-off. By using an orthogonal grating, broadband optical coupling into high-Q cavities of diverse geometric configurations can be achieved. As an example, the approach is applied to demonstrate over a 28-fold optical absorption enhancement across a 150 nm band around 900 nm wavelength in single-layer graphene embedded inside a Fabry–Perot cavity.

OCIS codes: (230.5750) Resonators; (140.3948) Microcavity devices; (230.1950) Diffraction gratings; (050.1950) Diffraction gratings.

http://dx.doi.org/10.1364/OL.40.002377

Optical resonant cavities, or optical resonators, are an important class of optical devices since they lead to resonant confinement of light in a small volume via the resonant cavity enhancement effect, thereby significantly boosting the effective optical path length and light–matter interactions (e.g., absorption, scattering, refraction, and light emission). Examples of devices capitalizing on the cavity enhancement effect include, but are not limited to: lasers, resonant-cavity light emitting diodes [1], cavity-enhanced photodetectors [2], resonator chemical and biological sensors [3], and resonant opticalmodulators [4].

In general, the strength of resonant cavity enhancement is characterized by two parameters: quality factor (Q-factor or Q) and finesse. A cavity with a high Q-factor and high finesse has minimal optical loss, and thus can sustain the resonant optical mode for an extended period of time, resulting in strong resonant cavity enhancement. Unfortunately, a high-Q or high finesse cavity's optical resonance also has a narrow spectral line width given by

$$\delta\lambda = \frac{\lambda}{Q} = \frac{\mathrm{FSR}}{F}, \tag{1}$$

where $\delta\lambda$ denotes the resonance line width in the wavelength domain, λ gives the resonant wavelength, Q is the Q-factor, FSR represents the cavity free spectral range, and F is the cavity finesse. The resonance line width inversely scales with Q and finesse, indicating that such strong resonant cavity enhancement is only accessible within a very limited wavelength range. The seemingly fundamental trade-off between line width and cavity enhancement places a major limitation on practical applications based on optical resonant cavities.

To overcome this limitation, several approaches have been attempted. A white light cavity (WLC), which has larger resonance line width than that of a conventional cavity, can be constructed by engineering the dispersion of the medium filling the cavity such that its group index vanishes. Such dispersion engineering is accomplished in atomic vapors with anomalous dispersion [5]. The attainable line width using this approach is limited by the dispersion characteristics of atomic vapors among other practical considerations [6]. Another approach to realize broadband resonance is to use chirped gratings with varying periods as reflectors for a Fabry–Perot (F-P) cavity [7,8]. The gratings are designed so that, when light is reflected, a wavelength-dependent phase shift that exactly compensates the round-trip phase delay difference at different wavelengths is acquired. A third approach involves using a pair of diffractive gratings to generate a wavelength-dependent path length difference in a cavity [9]. The approach, unfortunately, has been shown to be impractical because of the phase effect in optical diffraction [10]. As a last example, Matsko *et al.* devised an optical coupling scheme into whispering gallery mode (WGM) resonators [11]. The resonators are designed to support a swath of resonant modes closely spaced in the wavelength domain and, therefore, the coupling can be considered as quasi-continuous in wavelength.

Here we propose an alternative approach to enable broadband coupling into high-Q resonant cavities. The Letter is organized as follows: we start by describing the general broadband coupling principle which is applicable to a diverse cross section of resonator configurations. We subsequently examine grating-assisted coupling into F-P cavities as a specific implementation of the principle, and the key features of the coupling approach are discussed. Lastly, we apply the insight to demonstrate broadband absorption enhancement in single-layer graphene.

Without losing generality, we consider an optical resonant cavity whose resonant modes are confined along the cavity's longitudinal direction(s) and remain

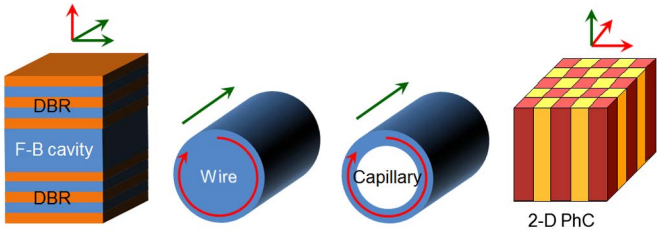

Fig. 1. Examples of optical cavity structures whose resonant modes are confined along the cavity's longitudinal direction(s) and remain unconfined in one or more transverse directions (from left to right): planar F-P cavity, micro-wire, micro-capillary, and two-dimensional photonic crystal cavity. The red arrows indicate the longitudinal directions and the green arrows label the transverse directions. Note that here we define the cavity mode propagation direction as the longitudinal direction, which corresponds to the azimuthal direction in the cases of wires and capillaries.

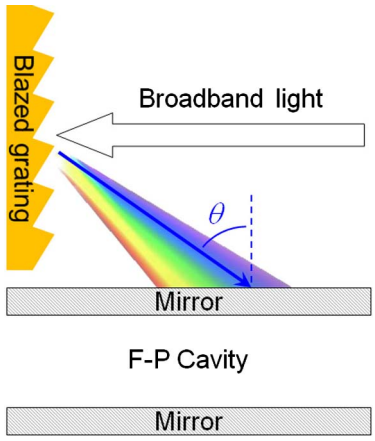

Fig. 2. Schematic illustration of broadband coupling configuration into an F-P cavity.

unconfined in one or more transverse directions. Figure 1 illustrates several examples of the resonant cavity structure. The resonance condition is then specified by the round-trip optical phase delay that equals integral multiples of wavelength along one of the longitudinal directions:

$$n_{\text{eff}}D + \frac{\varphi\lambda_l}{2\pi} = N\lambda_l, \tag{2}$$

where n_{eff} denotes the resonant mode effective index, D is the round-trip cavity physical length, φ represents phase shift associated with reflections at the cavity boundaries, λ_l is the wavelength along the longitudinal direction, and N is a positive integer. Equation (2) can be cast alternatively in terms of the longitudinal wave vector k_l at resonance

$$k_l = \frac{2\pi n_{\text{eff}}}{\lambda_l} = \frac{2\pi N - \varphi}{D}. \tag{3}$$

According to Eq. (3), the longitudinal wave vector k_l at resonance becomes wavelength independent provided that φ does not depend on the wavelength.

Now consider a broadband optical input having a vanishing wave vector along the cavity's longitudinal direction. When the optical input is incident on a diffractive element perpendicular to the incident light and with a reciprocal lattice vector $G = k_l$, the diffractive element imparts a longitudinal wave vector k_l to diffracted light. As a result, the diffracted light satisfies the resonance condition in Eqs. (2) and (3) and can efficiently couple into the resonant modes of the cavity. In other words, the longitudinal wave vector(s) remains invariant and always matches the reciprocal lattice vector of the diffractive element, whereas the transverse wave vector(s) changes to compensate for the wavelength variation.

The aforementioned broadband coupling principle is generically applicable to coupling into cavities whose resonant modes are not confined along the transverse direction(s). As a specific example, assume a resonant FP cavity composed of two parallel mirrors. The broadband coupling configuration illustrated in Fig. 2 is comprised of the cavity and a blazed grating perpendicular to the cavity mirrors. A polychromatic plane wave is incident in a direction parallel to the F-P cavity onto the grating, and its spectral components are split into different directions after diffraction. The angle of incidence θ for the first order diffracted light (measured with respect to the F-P cavity surface) is related to wavelength λ_θ by

$$\lambda_\theta = n\Lambda \cos\theta, \tag{4}$$

where n is refractive index of the medium surrounding the grating and Λ denotes the grating period. When the cavity is filled with the same medium, the angular dependence of an F-P cavity's resonant wavelength λ_θ is given by [12]

$$\lambda_\theta = \frac{4\pi nL\cos\theta}{2\pi N - \varphi_1 - \varphi_2}, \tag{5}$$

where L is the F-P cavity length and φ_1, φ_2 denotes the phase shifts at the two mirrors, respectively. Comparing Eqs. (4) and (5) provided that φ_1 and φ_2 are independent of incident angle and that the following condition is met:

$$\Lambda = \frac{4\pi L}{2\pi N - \varphi_1 - \varphi_2}, \tag{6}$$

broadband diffracted light can resonate inside the cavity. Equation (6) can also be written in terms of the longitudinal wave vector k_l as

$$k_l = \frac{2\pi}{\Lambda} = \frac{2\pi N - \varphi_1 - \varphi_2}{2L}, \tag{7}$$

which is equivalent to Eq. (3) noting that $D = 2L$.

Besides F-P etalon, the coupling scheme also applies to other cavity configurations with accessible transverse degrees of freedom. For example, if we consider a micro-capillary resonator shown in Fig. 1, a polychromatic input taking the form of a slab waveguide mode axially launched into the capillary wall can be coupled into the WGMs by a two-dimensional grating engraved on the capillary surface. The grating periods are specified by the equations

$$\frac{2\pi}{\Lambda_l} = k_l = \frac{2\pi N}{D} > k_0 \tag{8}$$

$$\Lambda_t < \frac{\pi}{n_{\text{eff}} k_0}, \tag{9}$$

where k_0 is the free-space wave vector, and Λ_l and Λ_t are the grating period along the longitudinal (azimuthal) and transverse (axial) directions, respectively. Equations (8) and (9) ensure that scattering into free space and backward propagating modes is suppressed and that the diffracted wave satisfies the resonant condition of the WGMs.

Here we want to highlight a few important features of the broadband coupling scheme:

(1) The broadband coupling scheme is fundamentally different from waveguide grating couplers, as the F-P cavity modes are not guided modes and phase matching along the in-plane direction is not required.

(2) Unlike classical WLC design which relies on dispersion engineering, the broadband coupling scheme equally applies even if material dispersion is present. This is evident from Eq. (3), as k_l depends on the cavity physical dimension and not the modal effective or group indices.

(3) The broadband coupling condition holds only when φ, the phase delay term in Eq. (3), is wavelength independent. The condition is automatically satisfied for most traveling wave resonators (micro-wires or micro-capillaries) as $\varphi = 0$; however, it warrants careful examination for standing wave cavities. One clear exception is an F-P cavity with metal-coated mirrors, as phase delay incurred by reflection on metal is a function of both wavelength and angle of incidence [13]. Even for dielectric distributed Bragg reflectors (DBRs or quarter wavelength stacks), φ is generally not a constant. To see that, we consider the phase delay $\varphi_{(i)}$ imparted by light propagation inside the i-th layer of the DBR, which is given by the product of the longitudinal (out-of-plane) wave vector $k_{l,i}$ in the layer (which is not conserved in refraction and therefore has to be labeled by the layer index) and the layer thickness, d_i:

$$\varphi_{(i)} = k_{l,i} d_i = \frac{2\pi n_i d_i}{\lambda_\theta} \cos\theta_i, \tag{10}$$

where n_i and θ_i is the refractive index and angle of incidence in the ith layer, respectively. In a quarter wavelength stack DBR mirror

$$n_i d_i = \frac{\lambda_{\theta=0}}{4} = \frac{\lambda_\theta}{4\cos\theta}. \tag{11}$$

Equation (10) can then be simplified to

$$\varphi_{(i)} = \frac{\pi}{2} \cdot \frac{\cos\theta_i}{\cos\theta}, \tag{12}$$

and θ_i and θ are connected by the Snell's law:

$$n_i \sin\theta_i = n \sin\theta. \tag{13}$$

Here n and θ is the cavity material index and angle of incidence as defined in Eqs. (4) and (5). Equations (12) and (13) indicate that $\varphi_{(i)}$ exactly equals $\pi/2$ only when $n_i = n$. When $n_i > n$, $\varphi_{(i)} > \pi/2$, and vice versa. Consequently, the transfer matrix associated with the DBR is no longer real or pure imaginary, as in the case of normal incidence, which confers an angle-dependent phase delay φ on the reflected wave.

A simple strategy to minimize the angular dependence of φ involves choosing a cavity material whose index situates between those of the high and low index layers composing the DBR so that the deviations from $\pi/2$ phase delay in the alternating layers cancel out each other. To illustrate this strategy, we examine the angle-dependent resonant wavelength for an F-P cavity whose resonance centers at $\lambda_{\theta=0} = 1$ μm at normal incidence. The symmetric cavity consists of a half-wavelength layer sandwiched between four pairs of alternating quarter wavelength layers with indices of $n_{\text{low}} = 1.5$ and $n_{\text{high}} = 3.0$. The cover, substrate, and cavity layer are all made of the same material with an index n. Figure 3 plots the angle-dependent s-polarization resonant wavelength simulated using the transfer matrix method. The red dot curve gives a cosine dependence of wavelength on incident angle as specified by Eqs. (4) and (5), which corresponds to the ideal broadband coupling condition. When $n = 1.66$ (the black solid line), the ideal cosine dependence is recovered with less than a 3 nm wavelength deviation across the entire 300 nm band.

(4) Another condition for the broadband coupling is that the optical input has a vanishing wave vector along the cavity's longitudinal direction, which is equivalent as stipulating that the incident wave has a planar wave front. In reality, the finite spatial extent of optical beams introduces a nonvanish longitudinal wave vector component and, consequently, limits coupling efficiency into high-Q modes. In the context of an F-P cavity shown in Fig. 2, an oblique incident beam laterally shifts away from its center after multiple reflections, which eventually precludes coherent amplitude buildup. In an F-P cavity, the reduction of coupling efficiency with

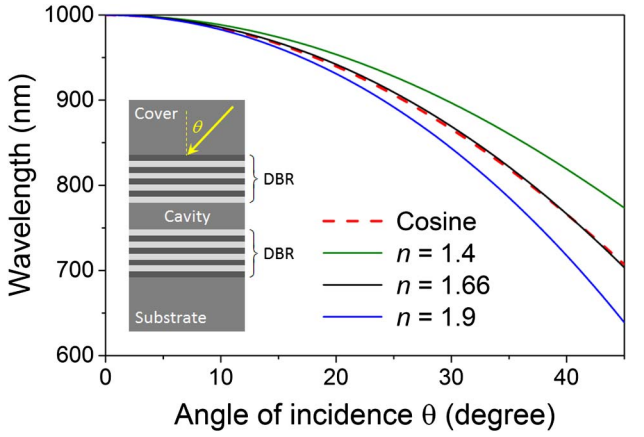

Fig. 3. Angular dependence of resonant wavelength in an F-P cavity: the ideal cosine dependence can always be attained by choosing an appropriate cavity material index n. The inset schematically illustrates the F-P cavity configuration.

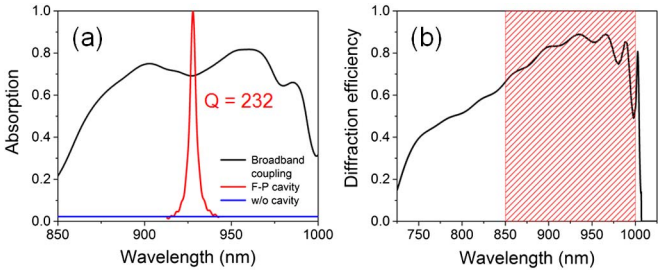

Fig. 4. (a) FDTD simulated absorption of TM-polarized light in a single layer graphene when freestanding (blue line), embedded in a critically coupled F-P cavity (red line), and configured in accordance with the broadband coupling scheme (black line); (b) diffraction efficiency of the blazed grating. The shaded region corresponds to the spectral domain shown in (a).

increasing Q poses a practical lower limit to the spot size semi-quantitatively given by the product $Q\lambda/2\pi$ [14].

The broadband coupling scheme described herein can be exploited to drastically boost the strength of light–matter interactions, for instance, optical absorption in graphene. In the absence of resonant enhancement, a single graphene layer absorbs only 2.3% of incident light [15]. A number of approaches have been proposed to enhance optical absorption in graphene leveraging guided mode resonance [16], waveguiding [17,18], resonant cavity enhancement [19,20], attenuated total internal reflection [21], and polaritons [22]. Most of these methods are either narrow-band, or cannot obtain near-unity absorption.

Here we demonstrate broadband optical absorption enhancement in graphene using the configuration shown in Fig. 2, where a monolayer graphene sheet is sandwiched in the middle of the F-P cavity. For the sake of computation efficiency, optical absorption in the graphene layer is calculated by taking the product of the wavelength-dependent grating diffraction efficiency and the coupling coefficient into the cavity, both simulated using two-dimensional finite-difference time-domain (FDTD) [23]. The modeling parameters are summarized in Table 1. Figure 4(a) compares the absorption of transverse magnetic (TM) polarized light in a single layer graphene when it is freestanding (blue curve), sandwiched inside a traditional F-P cavity at critical coupling (red curve), and placed in the broadband coupling configuration (black curve). The average absorption in graphene is 2.3%, 4.9%, and 65.3% over the 850–1000 nm band in these three cases, respectively; it is clear from the result that our coupling scheme significantly extends the bandwidth of cavity enhanced optical absorption. The fringes on the absorption spectra in the broadband coupling case mainly result from the wavelength dependence of the grating diffraction efficiency [Fig. 4(b)].

Table 1. Parameters Used for Modeling Graphene Absorption

λ_l	1 μm	DBR n_{low}	1.5
Λ	507 nm	DBR n_{high}	3
Blaze angle	23°	Cavity index	1.9875
Top mirror	4 pairs	n_{graphene}	[24]
Bottom mirror	10 pairs	n_{silver}	[25]

In summary, we analyzed a novel grating-assisted coupling scheme into optical cavities, where the bandwidth is not bound by the resonance linewidth. Using the design, we show that optical absorption in single layer graphene can be increased by 30 times over a wave band of 150 nm in the near infrared. The approach offers a facile route to enhance light–matter interactions without the conventional line width penalty, and thus may benefit applications such as sensing, switching, and photovoltaics.

References

1. R. G. Baets, D. Delbeke, R. Bockstaele, and P. Bienstman, Proc. SPIE **4996**, 74 (2003).
2. J. Wang, J. Hu, P. Becla, A. Agarwal, and L. C. Kimerling, Opt. Express **18**, 12890 (2010).
3. J. Hu, X. Sun, A. Agarwal, and L. C. Kimerling, J. Opt. Soc. Am. B **26**, 1032 (2009).
4. H. Lin, O. Ogbuu, J. Liu, L. Zhang, J. Michel, and J. Hu, J. Lightwave Technol. **31**, 4029 (2013).
5. G. S. Pati, M. Salit, K. Salit, and M. S. Shahriar, Phys. Rev. Lett. **99**, 133601 (2007).
6. H. N. Yum, X. Liu, P. R. Hemmer, J. Scheuer, and M. S. Shahriar, Opt. Commun. **305**, 260 (2013).
7. S. M. Shahriar, H. Yum, X. Liu, and P. Hemmer, *Frontiers in Optics 2011/Laser Science XXVII*, OSA Technical Digest (Optical Society of America, 2011), paper FThT7.
8. S. Loranger, M. Gagné, and R. Kashyap, Opt. Express **22**, 14253 (2014).
9. S. Wise, G. Mueller, D. Reitze, D. B. Tanner, and B. F. Whiting, Class. Quantum Grav. **21**, S1031 (2004).
10. S. Wise, V. Quetschke, A. J. Deshpande, G. Mueller, D. H. Reitze, D. B. Tanner, and B. F. Whiting, Phys. Rev. Lett. **95**, 013901 (2005).
11. A. Matsko, A. Savchenkov, and L. Maleki, "White-light whispering gallery mode optical resonator system and method," U.S. patent 7,515,786 (April 7, 2009).
12. P. Chamberlin, W. D. Pesnell, and B. Thompson, *The Solar Dynamics Observatory* (Springer, 2012), p. 295.
13. H. Macleod, *Thin-Film Optical Filters* (CRC Press, 2010).
14. J. De Merlier, K. Mizutani, S. Sudo, K. Sato, and K. Kudo, J. Lightwave Technol. **24**, 3202 (2006).
15. R. R. Nair, P. Blake, A. N. Grigorenko, K. S. Novoselov, T. J. Booth, T. Stauber, N. M. R. Peres, and A. K. Geim, Science **320**, 1308 (2008).
16. M. Grande, M. A. Vincenti, T. Stomeo, G. V. Bianco, D. de Ceglia, N. Aközbek, V. Petruzzelli, G. Bruno, M. De Vittorio, M. Scalora, and A. D'Orazio, Opt. Express **22**, 31511 (2014).
17. M. Liu, X. Yin, E. Ulin-Avila, B. Geng, T. Zentgraf, L. Ju, F. Wang, and X. Zhang, Nature **474**, 64 (2011).
18. H. Li, Y. Anugrah, S. J. Koester, and M. Li, Appl. Phys. Lett. **101**, 111110 (2012).
19. M. Furchi, A. Urich, A. Pospischil, G. Lilley, K. Unterrainer, H. Detz, P. Klang, A. M. Andrews, W. Schrenk, G. Strasser, and T. Mueller, Nano Lett. **12**, 2773 (2012).
20. M. Engel, M. Steiner, A. Lombardo, A. C. Ferrari, H. V. Löhneysen, P. Avouris, and R. Krupke, Nat. Commun. **3**, 906 (2012).
21. G. Pirruccio, L. Martín Moreno, G. Lozano, and J. Gómez Rivas, ACS Nano **7**, 4810 (2013).
22. B. Zhao, J. M. Zhao, and Z. M. Zhang, Appl. Phys. Lett. **105**, 031905 (2014).
23. Lumerical Solutions, Inc., http://www.lumerical.com/tcad-products/fdtd/
24. G. W. Hanson, J. Appl. Phys. **103**, 064302 (2008).
25. E. D. Palik, *Handbook of Optical Constants of Solids* (Academic, 1998).